ARMY RESEARCH LABORATORY

Modeling of Entangled Network Chains and Linear Solvent Chains in a Single-Chain Mean-Field Slip-Link Model

by Maria Katzarova, Yelena R. Sliozberg, Jan W. Andzelm, Randy A. Mrozek, Joseph L. Lenhart, and Jay D. Schieber

ARL-TR-6636 September 2013

NOTICES

Disclaimers

The findings in this report are not to be construed as an official Department of the Army position unless so designated by other authorized documents.

Citation of manufacturer's or trade names does not constitute an official endorsement or approval of the use thereof.

Destroy this report when it is no longer needed. Do not return it to the originator.

Army Research Laboratory

Aberdeen Proving Ground, MD 21005-5066

ARL-TR-6636 **September 2013**

Modeling of Entangled Network Chains and Linear Solvent Chains in a Single-Chain Mean-Field Slip-Link Model

Yelena R. Sliozberg, Jan W. Andzelm, Randy A. Mrozek, and Joseph L. Lenhart

Weapons and Materials Research Directorate, ARL

Maria Katzarova and Jay D. Schieber

Illinois Institute of Technology

Department of Physics

3440 S. Dearborn Street

Chicago, IL 60616

REPORT DOCUMENTATION PAGE	Form Approved OMB No. 0704-0188

1. REPORT DATE *(DD-MM-YYYY)*	2. REPORT TYPE	3. DATES COVERED (From - To)
September 2013	Final	June 2012–August 2012

4. TITLE AND SUBTITLE
Modeling of Entangled Network Chains and Linear Solvent Chains in a Single-Chain Mean-Field Slip-Link Model

5a. CONTRACT NUMBER

5b. GRANT NUMBER

5c. PROGRAM ELEMENT NUMBER

6. AUTHOR(S)
Maria Katzarova, Yelena R. Sliozberg, Jan W. Andzelm, Randy A. Mrozek, Joseph L. Lenhart, and Jay D. Schieber

5d. PROJECT NUMBER

5e. TASK NUMBER

5f. WORK UNIT NUMBER

7. PERFORMING ORGANIZATION NAME(S) AND ADDRESS(ES)
U.S. Army Research Laboratory
ATTN: RDRL-WMM-G
Aberdeen Proving Ground, MD 21005-5066

8. PERFORMING ORGANIZATION REPORT NUMBER
ARL-TR-6636

9. SPONSORING/MONITORING AGENCY NAME(S) AND ADDRESS(ES)

10. SPONSOR/MONITOR'S ACRONYM(S)

11. SPONSOR/MONITOR'S REPORT NUMBER(S)

12. DISTRIBUTION/AVAILABILITY STATEMENT
Approved for public release; distribution is unlimited.

13. SUPPLEMENTARY NOTES

14. ABSTRACT
Cross-linked polymer networks swollen with polymeric solvent have shown adaptive mechanical response. This frequency dependent response makes these gels desirable for applications such as tissue simulants for ballistic testing. This experimental observation is qualitatively modeled with the discrete slip-link model (DSM). Two applications of the DSM are used. First, an ideal entangled network (IEN) is modeled. This network is stoichiometrically cross-linked and no dangling ends, soluble sub-structures, or solvent are present. Secondly, the DSM is applied to these ideal entangled networks with solvent chains. This application is a coupling of two architectures: (1) entangled network chains (ENC) and (2) entangled solvent chains (ESC). The experimental system modeled is a stoichiometrically cross-linked polydimethylsiloxane (PDMS) network in the presence of high-molecular weight PDMS linear solvent. The network relaxation and flow behavior is predicted.

15. SUBJECT TERMS
Simulation, entangled polymer networks, slip-link model

16. SECURITY CLASSIFICATION OF:			17. LIMITATION OF ABSTRACT	18. NUMBER OF PAGES	19a. NAME OF RESPONSIBLE PERSON
a. REPORT	b. ABSTRACT	c. THIS PAGE			Jan W. Andzelm
Unclassified	Unclassified	Unclassified	UU	32	19b. TELEPHONE NUMBER (*Include area code*) (410) 306-4008

Contents

List of Figures

List of Tables

INTENTIONALLY LEFT BLANK.

1. Introduction

Cross-linked polymer networks swollen with polymeric solvent have shown adaptive mechanical response (*1*). This frequency-dependent response makes these gels desirable for applications such as tissue simulants for ballistic testing.

This experimental observation is qualitatively modeled with the discrete slip-link model (DSM) introduced by Schieber and Schieber et al. (*2, 3*) and further developed by Khaliullin and Schieber (*4–6*). Two applications of the DSM are used. First, an ideal entangled network (IEN), described by Jensen et al. (*7*), is modeled. This network is stoichiometrically cross-linked and no dangling ends, soluble sub-structures, or solvent chains are present. The entanglements are permanent (or trapped), since all chains are attached to the permanent network at the ends. Despite being trapped, relaxation through monomer shifting can occur between entanglements.

Secondly, the DSM is applied to these ideal entangled networks swollen with solvent chains. This application is a coupling of two architectures: (1) entangled network chains (ENCs) and (2) entangled solvent chains (ESCs). The experimental system modeled is a stoichiometrically cross-linked polydimethylsiloxane (PDMS) network in the presence of a high-molecular weight PDMS linear solvent. The network relaxation and flow behavior are predicted.

2. The Discrete Slip-Link Model

2.1 Ideal Entangled Network

As illustrated by references 7 and 8, the network chain can be described and coarse-grained by random walk statistics and modeled as a single-chain mean-field model. Entanglements define the primitive path of the chain. The parameters and variables of the coarse-grained chain are listed in table 1. In this application, Z, chosen from a distribution for a given chain, is constant since entanglements are trapped in the IEN model. Monomer density, N_i, fluctuates due to Kuhn step shuffling through the slip-links in the sliding dynamics (SD) process.

Table 1. Parameters and variables of the coarse-grained chain.

	Description
Parameters	
N_{K}^{γ}	Total number of Kuhn steps*
β	Entanglement spacing parameter
τ_{K}	Average time of transferring one Kuhn step through an entanglement
Variables	
Z	Number of entangled strands
N_i	Number of Kuhn steps in strand i
$\mathbf{Q}_i$	Orientation vector between entanglements i and $i+1$
τ_i^{CD}	Characteristic lifetime of i entanglement determined by constraint dynamics (CD)

*$\gamma \equiv$ N, S indicates that we can work with two different molecular weights in the second model application.

The random walk of N_i Kuhn steps in a strand between two entanglements with a connector vector, $\boldsymbol{Q_i}$, has a Gaussian free energy given by

$$\frac{F_s(\boldsymbol{Q}_i, N_i)}{k_B T} = \frac{3\boldsymbol{Q}_i^2}{2N_i a_{\mathrm{K}}^2} + \frac{3}{2}\ln\left[\frac{2\pi N_i a_{\mathrm{K}}^2}{3}\right], \tag{1}$$

where k_B is the Boltzmann constant and T is the temperature. The free energy of the network chain (NC) composed of Z strands is a sum of the free energies associated with the entangled strands:

$$F_{\mathrm{NC}}(\Omega) = \sum_{i=1}^{Z} F_s(\boldsymbol{Q}_i, N_i), \tag{2}$$

where $\Omega \equiv (Z, \{N_i\}, \{\boldsymbol{Q_i}\}, \{\tau_i^{\mathrm{CD}}\})$ is the cross-linked chain conformation. The equilibrium distribution of such a chain is given by the modified Maxwell-Boltzmann relation (*5*)

$$p_{eq}^{\gamma}(\Omega) = \frac{\delta(N_{\mathrm{K}}^{\gamma}, \sum_{i=1}^{Z} N_i)}{J}\exp\left[-\frac{F(\Omega)}{k_B T}\right]\exp\left[\frac{\mu^E(Z-1)}{k_B T}\right]\prod_{i=1}^{Z-1} p^{\mathrm{CD}}(\tau_i^{\mathrm{CD}}), \tag{3}$$

where $p^{\mathrm{CD}}(\tau_i^{\mathrm{CD}})$ is the probability density for the i^{th} entanglement with a characteristic CD lifetime, τ_i^{CD}, determined by CD. It is determined self-consistently from the destruction of entanglements in a system by SD. Entanglements between two ENCs will never be destroyed by CD; hence, τ_i^{CD} is infinitely large and for those $p^{\mathrm{CD}}(\tau^{\mathrm{CD}}) = 2\delta(1/\tau^{\mathrm{CD}})/(\tau^{\mathrm{CD}})^2$. The Kronecker delta function $\delta(i,j) := \delta_{i,j}$ is responsible for the conservation of Kuhn steps in a chain and $J = (1+1/\beta)^{N_K^{\gamma}-1}$ is the normalization constant. The entanglement chemical potential of the

surrounding chains, μ_E, is responsible for fluctuations in the number of entanglements on the chain.

2.2 Entangled Network Chains and Entangled Solvent Chains

We combine two architectures of chains: one for ENCs and one for ESCs. The solvent chains will have two free-ends where entanglements can be created and destroyed by SD, while some fraction of entanglements can be created and destroyed anywhere on the strand by CD. This latter process is caused by the SD of surrounding solvent chains. While still another fraction of entanglements cannot be created or destroyed by CD, as these are entangled with the network chains and they are trapped. The ENC will have a fraction of entanglements created and destroyed by CD due to entanglements with ESC.

2.3 Stress Relaxation of Network Chains and Solvent Chains

The stress tensor is obtained from the chain free energy

$$\boldsymbol{\tau_\gamma}(t) = -n_\gamma \left\langle \sum_{i=1}^{Z} \boldsymbol{Q}_i \left(\frac{\partial F(\boldsymbol{\Omega})}{\partial \boldsymbol{Q}_i} \right)_{T,\{N_i\},\{\boldsymbol{Q}_{j\neq i}\}} \right\rangle_\gamma , \tag{4}$$

where $\langle ... \rangle$ is an ensemble average. The relaxation modulus, $G_\gamma(t)$, is obtained using the Green-Kubo expression

$$G_\gamma(t) = \frac{1}{n_\gamma k_B T} \left\langle \tau_{xy}(0)\tau_{xy}(t) \right\rangle_{\mathrm{eq},\gamma} , \tag{5}$$

The subscript γ is either "NC" or "SC" for solvent chain. The relaxation modulus for each structure, G_{NC} and G_{SC} is obtained from Green-Kubo simulations of the two ensembles, while G(t) for the combined system is a linear superposition of the relaxation moduli of the two components

$$G(t) = w_{NC} G_{NC}(t) + w_{SC} G_{SC}(t), \tag{6}$$

where w_{NC} and w_{SC} is the volume fraction of network chains and solvent chains, respectively. The network chains and solvent chains influence each other through CD.

2.4 Equilibrium Dynamics for ENC and ESC

At equilibrium, Kuhn step shuffling between entangled strands is due to Brownian forces and free energy differences. The evolution equation for the probability density describing the

conformation of a chain is given by the Chapman-Kolmogorov equation (*2*)

$$\frac{\partial p(\Omega, t \mid \Omega_0, t_0)}{\partial t} = -\sum_{i=1}^{Z} \frac{\partial}{\partial \boldsymbol{Q_i}} \cdot [\boldsymbol{\kappa} \cdot \boldsymbol{Q_i}] p(\Omega, t \mid \Omega_0, t_0) + \int W(\Omega \mid \Omega') p(\Omega', t \mid \Omega_0, t_0) d\Omega' - \int W(\Omega' \mid \Omega) p(\Omega, t \mid \Omega_0, t_0) d\Omega', \quad (7)$$

where $\boldsymbol{\kappa} := (\nabla \boldsymbol{v})^\dagger$ is the transpose of the velocity gradient. We assume affine entanglement and cross-link motion, $d\boldsymbol{Q}_i/dt = \boldsymbol{\kappa} \cdot \boldsymbol{Q}_i$. The probability density of having conformation Ω at time t given that at t_0 the conformation was Ω_0 is $p(\Omega, t \mid \Omega_0, t_0)$. The function $W(\Omega \mid \Omega')$ is the transition probability from conformation Ω to conformation Ω' per unit time and has five contributions

$$W = \left(\sum_{i=1}^{Z-1} W_{\mathrm{sh}}^i \right) + W_{\mathrm{d}}^{\mathrm{SD}} + W_{\mathrm{c}}^{\mathrm{SD}} + W_{\mathrm{d}}^{\mathrm{CD}} + W_{\mathrm{c}}^{\mathrm{CD}}, \quad (8)$$

where W_{sh}^i is the transition rate probability for Kuhn-step shuffling through entanglement i. $W_{\mathrm{d}}^{\mathrm{SD}}$ and $W_{\mathrm{c}}^{\mathrm{SD}}$ represent destruction and creation of the entanglements on the end of the solvent chain due to SD (these terms are zero in the IEN and ENC models), and $W_{\mathrm{d}}^{\mathrm{CD}}$ and W_c^{CD} represent destruction and creation of the entanglements anywhere on the strand due to CD (these last two contributions are zero in the IEN model). When deriving expressions for the transition probability, we satisfy detailed balance

$$W(\Omega' \mid \Omega) = W(\Omega \mid \Omega') \frac{p_{\mathrm{eq}}(\Omega')}{p_{\mathrm{eq}}(\Omega)} \quad (9)$$

Details of these transition probabilities can be found in Jensen et al. (*7*). It is assumed that cross-links are fixed in space.

2.5 Constraint Dynamics Spectrum

It is necessary to obtain a CD spectrum $p^{\mathrm{CD}}(\tau)$ such that, by assuming binary entanglements, the destruction of entanglements by SD and CD will be equal in time. This can be done by keeping track of the entanglements from their individual time of creation to their individual time of destruction. By doing this, we weight short-lived entanglements more than long-lived ones.

This gives us the cumulative distribution of lifetimes, $\mathbb{P}(t)$, related to $p^{\mathrm{CD}}(\tau^{\mathrm{CD}})$ through

$$\begin{aligned} f_d(t) &= 1 - \mathbb{P}(t) \\ &= \frac{\int_0^\infty \frac{p^{\mathrm{CD}}(\tau^{\mathrm{CD}})}{\tau^{\mathrm{CD}}} \exp\left(-\frac{t}{\tau^{\mathrm{CD}}}\right) d\tau^{\mathrm{CD}}}{\int_0^\infty \frac{p^{\mathrm{CD}}(\tau^{\mathrm{CD}})}{\tau^{\mathrm{CD}}} d\tau^{\mathrm{CD}}} \\ &= \frac{\int_0^\infty \frac{p_{\mathrm{SC}}^{\mathrm{CD}}(\tau^{\mathrm{CD}})}{\tau^{\mathrm{CD}}} \exp\left(-\frac{t}{\tau^{\mathrm{CD}}}\right) d\tau^{\mathrm{CD}}}{\int_0^\infty \frac{p_{\mathrm{SC}}^{\mathrm{CD}}(\tau^{\mathrm{CD}})}{\tau^{\mathrm{CD}}} d\tau^{\mathrm{CD}}}, \end{aligned} \tag{10}$$

because $\int_0^\infty \delta(1/\tau)/\tau^3 d\tau = 0$.

Since we later compare the theory with experimental PDMS data, we perform simulations with $N_{\mathrm{K}} = 307$ and $\beta = 25.3$. The estimate of these parameters is described in section 3. The resulting $f_d(t)$ from a solvent chain simulation without CD is shown in figure 1.

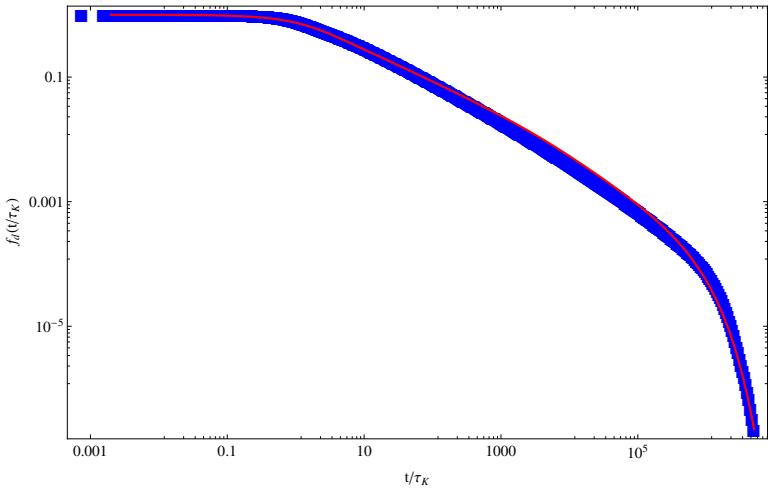

Figure 1. $f_d(t)$ obtained from a simulation of solvent chains with $N_{\mathrm{K}} = 307$ and $\beta = 25.3$ and an ensemble of 100 chains. The crosses are simulated data, while the *full line* is a fitted spectrum: $\tau_0 = 1$, $\tau_1 = 5000$, $\tau_2 = 1000000$, $\alpha_1 = 0.5$, and $\alpha_2 = 0.3$.

The following spectrum is used to fit well the CD normalized lifetime distribution probability of an ideal entangled network with solvent chains:

$$p^{\mathrm{CD}}(\tau) = w_{\mathrm{SC}} \left(\frac{\tau^{\alpha_1 - 1} H(\tau - \tau_0) H(\tau_1 - \tau)}{\frac{\tau_1^{\alpha_1} - \tau_0^{\alpha_1}}{\alpha_1} + \frac{\tau_2^{\alpha_2} - \tau_1^{\alpha_2}}{\alpha_2} \tau_1^{\alpha_1 - \alpha_2}} + \frac{\tau^{\alpha_2 - 1} H(\tau - \tau_1) H(\tau_2 - \tau) \tau_1^{\alpha_1 - \alpha_2}}{\frac{\tau_1^{\alpha_1} - \tau_0^{\alpha_1}}{\alpha_1} + \frac{\tau_2^{\alpha_2} - \tau_1^{\alpha_2}}{\alpha_2} \tau_1^{\alpha_1 - \alpha_2}} \right) + w_{\mathrm{NC}} \frac{2\delta(1/\tau)}{\tau^2}. \tag{11}$$

The delta function assigns an infinite lifetime to a fraction w_{NC} of entanglements.

3. Results

3.1 BSW Spectrum

To estimate the Fourier transform of $G(t)$, we fit the simulated data with a mathematical expression given by

$$G(t) = (G_N^0 - G_0) \int_0^\infty \frac{h(\tau)}{\tau} \exp\left(-\frac{t}{\tau}\right) d\tau + G_0 \tag{12}$$

where G_N^0 is the entanglement plateau and G_0 is the equilibrium plateau and $h(\tau)$ a modified Baumgaertel, Schausberger, and Winter (BSW) spectrum (*9*)

$$h(\tau) = \frac{\sum_{i=1}^{m} \tau^{\alpha_i} H(\tau_{i-1} - \tau) H(\tau - \tau_i) \prod_{j=1}^{i-1} \tau_j^{\alpha_j - \alpha j + 1}}{\sum_{i=1}^{m} \frac{\tau_i^{\alpha_i} - \tau_{i-1}^{\alpha_i}}{\alpha_i} \prod_{j=1}^{i-1} \tau_j^{\alpha_j - \alpha_{j+1}}}. \tag{13}$$

The fit is performed by minimizing the χ^2 function assuming constant relative error

$$\chi^2 := \sum_{i=0}^{N-1} \left(\frac{f_i - g(x_i)}{\sqrt{f_i}} \right)^2 \tag{14}$$

where f_i is the numerical value obtained at x_i point and $g(x_i)$ is the analytical function that is used to fit the data. For the IEN results, we fit only one mode, and equation 5 reduces to

$$h(\tau) = \frac{\alpha \tau^\alpha}{\tau_1^\alpha - \tau_0^\alpha} H(\tau_1 - \tau) H(\tau - \tau_0) \tag{15}$$

where τ_1 and τ_0 are the longest and shortest relaxation times, respectively.

To transform between the experimental time domain to the frequency regime, a one-sided Fourier transform is used, $G^*(\omega) := i\omega\bar{\mathcal{F}}\{G(t)\}$

3.2 DSM Parameters

To calculate the relaxation modulus, experimental parameters are necessary including the molecular weight of the polymer and Kuhn length, M_W and M_K, respectively; polymer density, ρ; plateau modulus, G_N^0; and temperature, T. The data for the system are presented in table 2. The polydispersity index, M_W/M_N, is also given as a measure of the quality of the melt.

Table 2. Experimental data for PDMS.

Name	M_W (kg/mol)	M_K (kg/mol)	M_W/M_N	ρ (g/cm^3)	T (K)	G_N^0 (kPa)
T314	314.3	0.381	1.15	0.965	293	227
Reference	(***?***)	(***?***)	(*?*)	(*?*)	(*?*)	(*?*)

The two input parameters for the DSM model are the number of Kuhn segments, N_K, and the model parameter, β. N_K can be calculated using $N_\mathrm{K} = M_W/M_\mathrm{K}$. The data in Ressia et al. (*10*) are used to find β by fitting the Fourier transform of the following expression to it:

$$G(t) = G_N^0 \int_0^\infty \frac{h(\tau)}{\tau} \exp\left(-\frac{t}{\tau}\right) d\tau \tag{16}$$

where G_N^0 is taken from Khaliullin and Schieber (*5*)

$$G_N^0 = \frac{\rho RT}{M_W}\left(\left(\frac{\beta}{\beta+1}\right)^{N_\mathrm{K}-1} + \frac{N_\mathrm{K}-\beta-2}{\beta+1}\right) \tag{17}$$

The results are shown in figure 2.

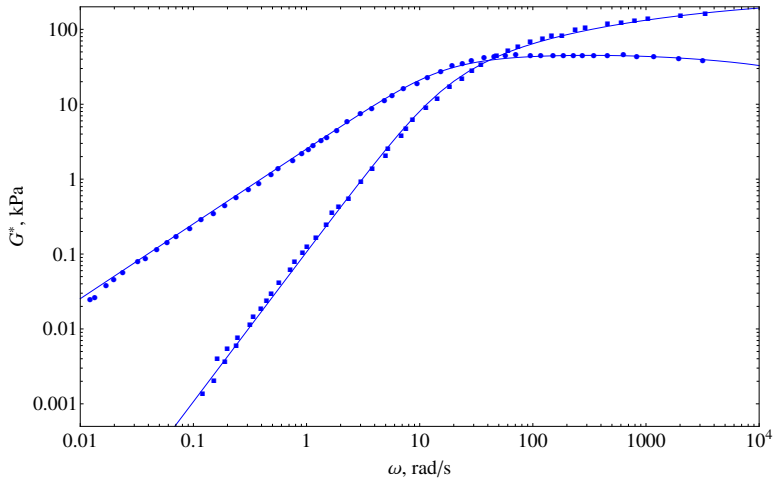

Figure 2. T314 blue symbols are experimental data from Ressia et al. (*10*) fitted with a two mode BSW spectrum.

With these parameters and following the procedure outlined in Chantawansri et al. (*8*), the relaxation modulus is transformed to the frequency domain and compared with data as seen in figure 3. τ_{K} was also retrieved when this fit to the experimental data was done.

The values for the two parameters are shown in table 3

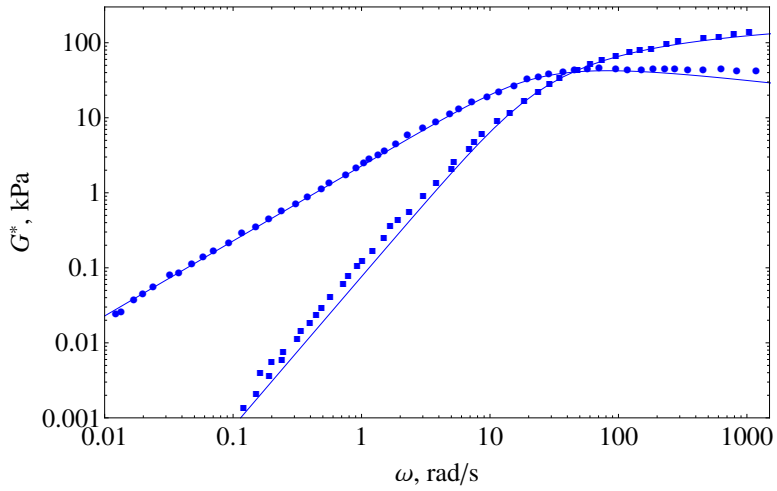

Figure 3. T314 blue symbols are experimental data and the line is the DSM prediction with $\tau_{\mathrm{K}} = 0.002\mu s$.

Table 3. Parameters needed for DSM program.

Name	N_{K}	β	τ_{K}
T314	825	25.3	$0.002\mu s$

3.3 Ideal Entangled Network

In the ideal network, we have only trapped entanglements.

In figure 4, we show the Green-Kubo results of simulating 100 IEN chains for $N_{\mathrm{K}} = 307$ and $\beta = 25.3$. The results are normalized with the entanglement plateau modulus, which is determined analytically as (*2, 3, 5*)

$$\frac{G_N^0}{\rho RT/M} = \langle Z \rangle_{\mathrm{eq}} = \frac{N_{\mathrm{K}} + \beta}{\beta + 1} \tag{18}$$

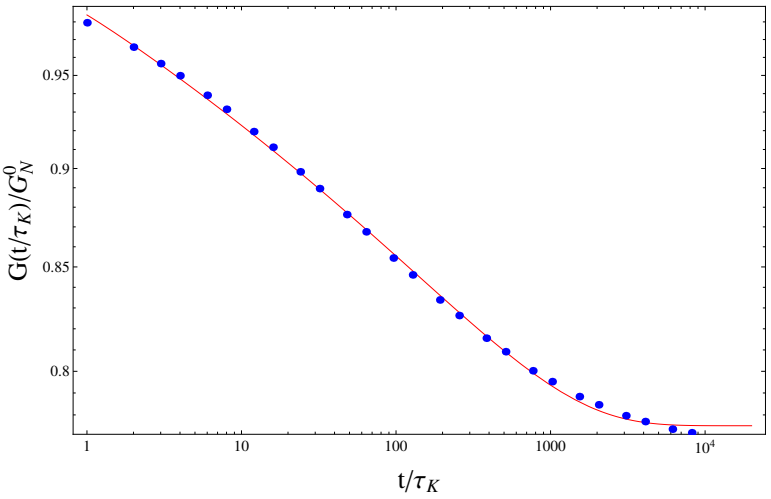

Figure 4. Relaxation modulus produce by the IEN model with $N_{\mathrm{K}} = 307$ and $\beta = 25.3$. The red line is the BSW fit of the DSM prediction.

The resulting G^* spectrum, for $N_{\mathrm{K}} = 307$ and $\beta = 25.3$, is shown in figure 5. The difference in magnitude of G' and G'' makes it difficult to see the shape of G', which is rendered in the blow up in the figure inset, revealing the three frequency regimes. The BSW parameters are listed in table 4.

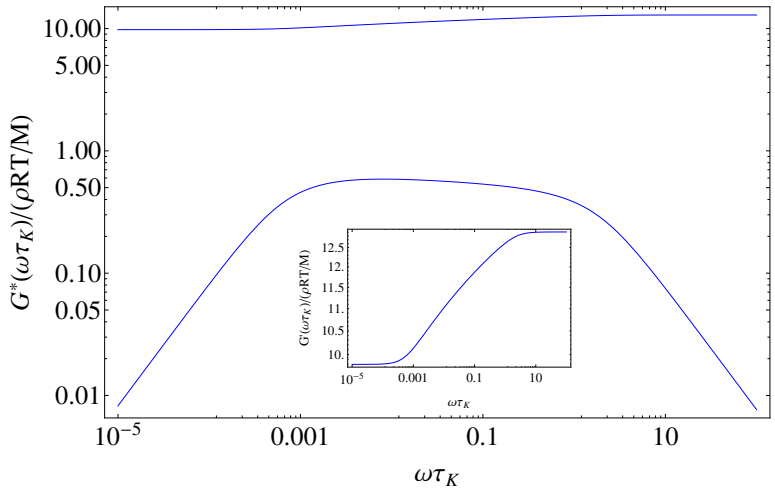

Figure 5. Dynamic relaxation spectrum for $N_{\mathrm{K}} = 307$ and $\beta = 25.3$ obtained with the IEN model. G' is several orders of magnitude larger than G''; the shape of G' can be seen in the *inset*.

As discussed by Jensen et al. (*7*), experimental observations of stoichiometrically imbalanced networks show that G'' and G' are of the same order of magnitude at intermediated frequencies; the DSM suggests that energy dissipation is largely a result of the dangling ends and soluble structures.

Table 4. BSW parameters obtained by fitting equation 6 combined with equation 4 to the DSM prediction presented in figure 2.

N_{K}	β	G_0	α	τ_0	τ_1
307	25.3	7.5426	0.0141	0.5	2706

3.4 Entangled Network with Solvent Chains

The DSM is used to qualitatively capture the trends of experimental data at times scales slower than glassy modes. For a quantitative description, better characterization of network structure and solvent polydispersity is required. An example of experimental data is shown in figure 6 (*1*).

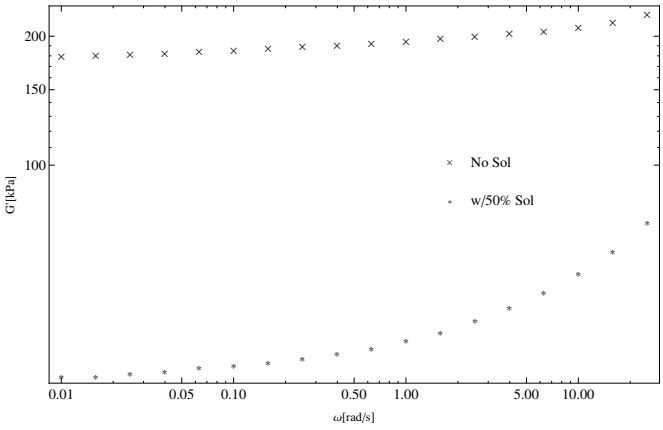

Figure 6. G' for a PDMS gel containing 50% solvent of molecular weight 139,000 g/mol.

We simulate network chains and solvent chains with the same parameters, i.e., $N_{\mathrm{K}} = 307, \beta = 25.3$, and $w_{\mathrm{SC}} = 0.1$. The Green-Kubo results from these simulations are shown in figure 7 together with the corresponding G_{IEN} obtained in the previous section. The length of time for relaxation increases in the presence of solvent chains, as expected. When compared, G_{NC} clearly shows the CD effect in comparison to G_{IEN} where G_0 is reached much quicker and is increased. The presence of solvent chains increases G_N^0. The analytic expression for G_N^0 is

$$\begin{aligned} \frac{G_N^0}{\rho RT/M_{\mathrm{K}}} &= \frac{w_{\mathrm{NC}}}{N_{\mathrm{K}}^{\mathrm{N}}} \left\langle Z_{\mathrm{ENC}} \right\rangle_{\mathrm{eq}} + \frac{w_{\mathrm{SC}}}{N_{\mathrm{K}}^{\mathrm{S}}} \left(\left\langle Z_{\mathrm{ESC}} \right\rangle_{\mathrm{eq}} - 1 \right) \\ &= \frac{w_{\mathrm{NC}}}{N_{\mathrm{K}}^{\mathrm{N}}} \frac{N_{\mathrm{K}}^{\mathrm{N}} + \beta}{\beta + 1} + \frac{w_{\mathrm{SC}}}{N_{\mathrm{K}}^{\mathrm{S}}} \left(\frac{N_{\mathrm{K}}^{\mathrm{S}} + \beta}{\beta + 1} - 1 \right) \end{aligned} \tag{19}$$

M_{K} is the molecular weight of a Kuhn step while $\left\langle Z_{\mathrm{ENC}} \right\rangle_{\mathrm{eq}}$ and $\left\langle Z_{\mathrm{ESC}} \right\rangle_{\mathrm{eq}}$ are the average number of entangled chains for the network and solvent chains, respectively, while $N_{\mathrm{K}}^{\mathrm{N}}$ and $N_{\mathrm{K}}^{\mathrm{S}}$ are the total number of Kuhn steps in the network chains and solvent chains, respectively. The top horizontal line in figure 7 is an analytic estimate of the plateau modulus, $G_{0,\mathrm{NC}}$ given by

$$\frac{G_{0,\mathrm{NC}}}{\rho RT/M} = 0.74 Z_{\mathrm{T}} + 1 \tag{20}$$

Z_{T} is the average number of trapped entanglements:

$$Z_{\mathrm{T}} = w_{\mathrm{NC}} \left(\left\langle Z_{\mathrm{ENC}} \right\rangle \mathrm{eq} - 1 \right). \tag{21}$$

The bottom horizontal line in figure 7 represents the estimated analytic plateau modulus, $G_{0,ana}$, of the network with solvent chains, given by

$$\frac{G_{0,\mathrm{ana}}}{\rho RT/M} = w_{\mathrm{NC}} \frac{G_{0,\mathrm{NC}}}{\rho RT/M} = w_{\mathrm{NC}}(0.74Z_{\mathrm{T}} + 1). \tag{22}$$

These later two equations suggest the G_0 is a function of trapped entanglements only.

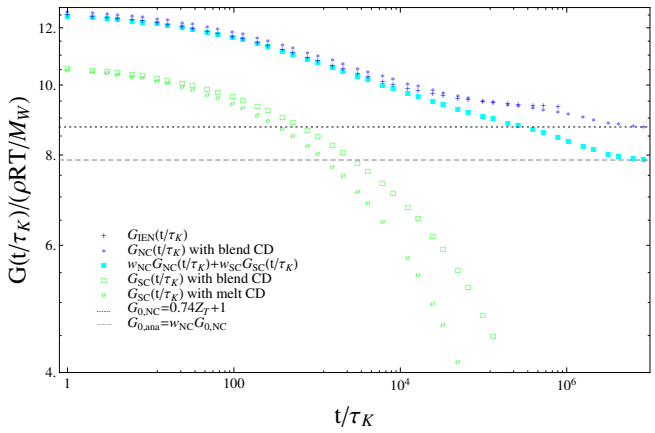

Figure 7. Green-Kubo simulation results.
$N_{\mathrm{K}}^{\mathrm{N}} = N_{\mathrm{K}}^{\mathrm{S}} = 307$, $\beta = 25.3$, and $w_{\mathrm{SC}} = 0.1$.

$G(t)$ for the blend is fit again as described previously and converted into the frequency domain as shown in figure 8.

Figure 8 shows the G^* result, and it is seen that G' and G'' are becoming closer in order of magnitude compared to the ideal entangled network with no entangled solvent present. A qualitative comparison of this result with experimental data from Mrozek et al. (*1*) is shown in figure 9.

A number of assumptions listed in Jensen et al. (*7*) related to requiring better characterization of the experimental network and solvent chains, suggest an explanation regarding the discrepancy between the DSM prediction and the data. Additionally, a comparison with experimental polydisperse solvent, which is used for results in the next section, and the DSM prediction of the same monodisperse solvent is shown in figure 10, making apparent an effect of polydispersity on mechanical properties.

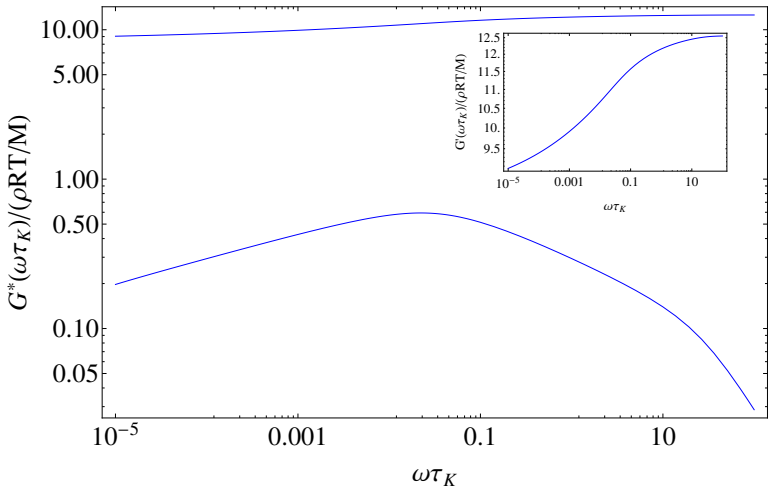

Figure 8. G^* result for $N_{\mathrm{K}}^{\mathrm{N}} = N_{\mathrm{K}}^{\mathrm{S}} = 307$, $\beta = 25.3$, and $w_{\mathrm{SC}} = 0.1$.

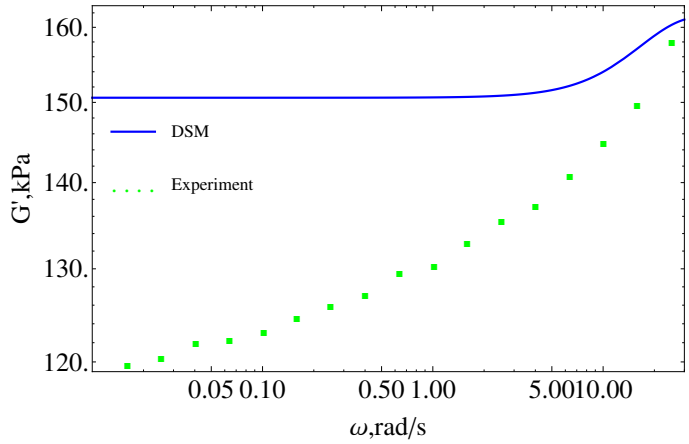

Figure 9. DSM prediction for PDMS, $N_{\mathrm{K}}^{\mathrm{N}} = N_{\mathrm{K}}^{\mathrm{S}} = 307$, $\beta = 25.3$ and $w_{\mathrm{SC}} = 0.1$ and experimental data for a network (117 kDa, PDI=1.55) with 10% polydisperse 139 kDa solvent.

3.5 Simple Elongation of Ideal Entangled Network with Solvent Chains

The DSM is used to predict the mechanical response of an ideal entangled network swollen with monodisperse entangled solvent. For a simple pull test for constant elongation rate of 5 in/sec with an initial sample length of 1 in, the elongation ratio, λ ($\lambda = l/L$), is given by

$$\lambda = \dot{\lambda} t + 1 \tag{23}$$

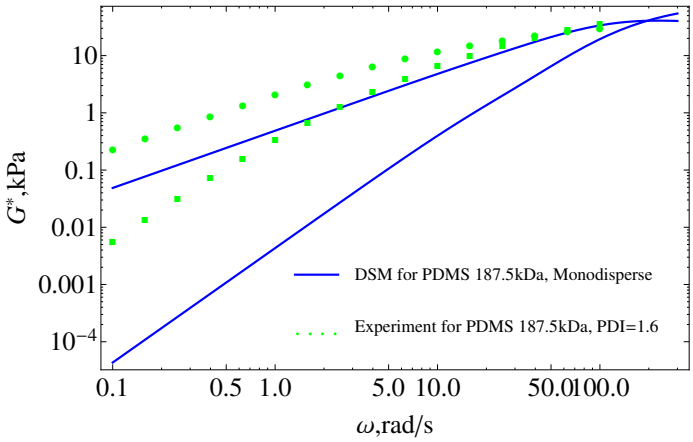

Figure 10. DSM prediction for monodisperse solvent, $N_K^S = 492$, $\beta = 25.3$, and PDMS experimental data, 187.5 kDa, PDI=1.6.

where $\dot{\lambda} = 5$ 1/s. For the DSM, the elongation ratio is related to the logarithmic (Hencky) strain, which is used by the algorithm, by

$$\epsilon = \log(\lambda) \tag{24}$$

and consequently the true strain rate can be expressed as

$$\dot{\epsilon} = \frac{\dot{\lambda}}{\dot{\lambda}t + 1} = \frac{1}{t + 1/\dot{\lambda}} \tag{25}$$

For the melt component of the system, the longest relaxation time is, $\tau_d = 0.03$ s, obtained from Sliozberg et al. (*12*). The resulting Weissenberg number, $Wi = \dot{\epsilon}\tau_d$, is pictured in figure 11.

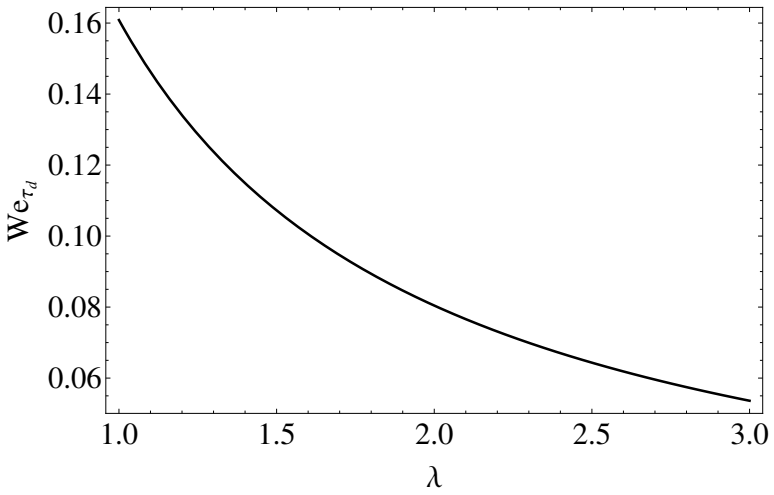

Figure 11. Weissenberg number for uniaxial extension for PDMS melt, 187.5 kDa, $\dot{\lambda} = 5$ 1/s, $\tau_d = 0.03$ s.

This result is consistent with the DSM prediction, shown in figure 12, which shows that the solvent chains are not experiencing nonlinear deformation. For this system, the main contribution to the stress is from the network component. The system response is a weighted average of the network and solvent stress, depicted by the blend prediction. To further illustrate this minimal contribution to stress from the melt, an additional result is plotted in figure 12 for a prediction of just 50% network solution diluted with non-entangled ideal solvent, for which $\beta^{solution} = 50.6$ was calculated using a scaling argument regarding the entanglement spacing for a polymer chain in solution according to

$$\beta^{solution} = \frac{\beta^{melt}}{\phi} \tag{26}$$

where ϕ is the volume fraction of the network. It can be seen that the two results are very nearly the same.

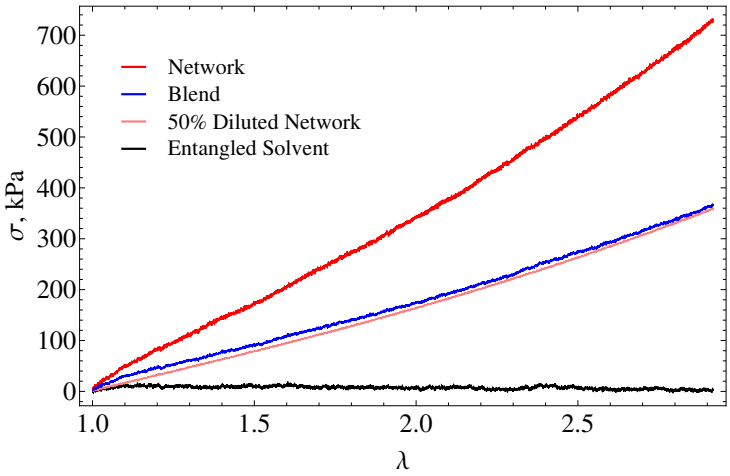

Figure 12. True stress, σ, vs. stretch ratio, λ for uniaxial tension ($\dot{\lambda} = 5$ 1/s) using the DSM for $N_{\mathrm{K}}^{\mathrm{N}} = 307$, $N_{\mathrm{K}}^{\mathrm{S}} = 492$, $\beta = 25.3$, and $w_{\mathrm{SC}} = 0.5$. For the diluted network, $\beta^{solution} = 50.6$, $N_{\mathrm{K}}^{\mathrm{N}} = 307$.

A qualitative comparison with experimental data from Sliozberg et al. (*12*) is shown in figure 13. Again, characterization of network architecture and solvent polydispersity is necessary for a quantitative comparison. Both of these latter features could work to bring down the prediction of stress approximately 0.57 times making the agreement better as can be seen in the figure.

In a Mooney plot, shown in figure 14, for the DSM predicted ideal system and the experimental system, a linear mechanical system response can be seen.

4. Conclusions

Two applications of the discrete slip-link model have been presented. The first is used to model ideal entangled networks. The other application of the model is a combination of ENCs and ESCs. As a starting point, equilibrium and flow experimental data were described qualitatively, and for simplicity, network chains and solvent chains were assumed monodisperse, linear, and of the same molecular weight. Additional detailed characterization of the network and melt is necessary to make quantitative predictions.

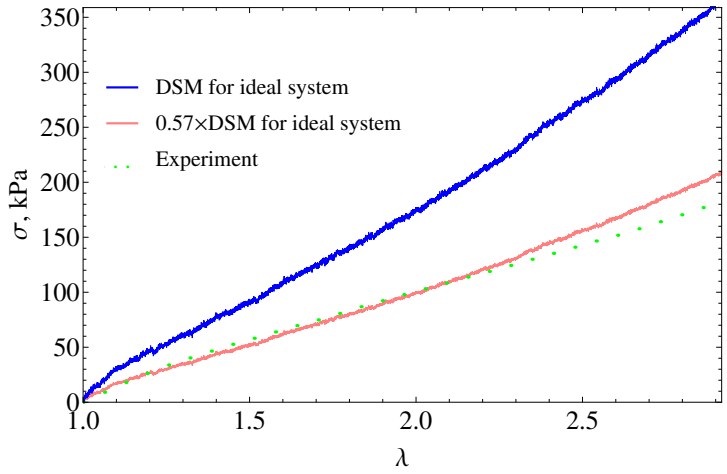

Figure 13. True stress, σ, vs. stretch ratio, λ for uniaxial tension ($\dot{\lambda} = 5$ 1/s) using the DSM for $N_{\mathrm{K}}^{\mathrm{N}} = 307$, $N_{\mathrm{K}}^{\mathrm{S}} = 492$, $\beta = 25.3$, and $w_{\mathrm{SC}} = 0.5$. Experimental data from Sliozberg et al. (*12*) for $\dot{\lambda} = 5$ 1/s, containing 50% T204.

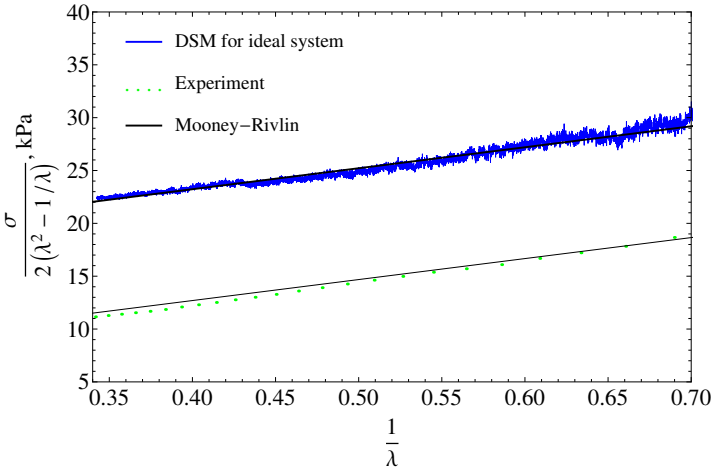

Figure 14. Mooney plot for experimental data from Sliozberg et al. (*12*) for $\dot{\lambda} = 5$ 1/s, containing 50% T204 and DSM prediction for $N_{\mathrm{K}}^{\mathrm{N}} = 307$, $N_{\mathrm{K}}^{\mathrm{S}} = 492$, $\beta = 25.3$, and $w_{\mathrm{SC}} = 0.5$ for uniaxial tension ($\dot{\lambda} = 5$ 1/s).

5. References

1. Mrozek, R. A.; Cole, P. J.; Otim, K. J.; Shull, K. R.; Lenhart, J. L. Influence of Solvent Size on the Mechanical Properties and Rheology of Polydimethylsiloxane-based Polymeric Gels. *Polymer* **2011**, *52*, 3422–3430.

2. Schieber, J. Fluctuations in Entanglements of Polymer Liquids. *Journal of Chemical Physics* **2003**, *18* (11), 5162–5166.

3. Schieber, J.; Neergaard, J.; Gupta, S. A Full-chain, Temporary Network Model with Sliplinks, Chain-length Fluctuations, Chain Connectivity and Chain Stretching. *Journal of Rheology* **2003**, *47* (1), 213–233.

4. Khaliullin R.; Schieber J. Analytic Expressions for the Statistics of the Primitive-path Length in Entangled Polymers. *Physical Review Letters* **2008**, *100* (18), 188302–188304.

5. Khaliullin R.; Schieber J. Self-consistent Modeling of Constraint Release in a Single-chain Mean-field Slip-link Model. *Macromolecules* **2009**, *42* (19), 7504–7517.

6. Khaliullin R.; Schieber J. Application of the Slip-link Model to Bidisperse Systems. *Macromolecules* **2010**, *43*, 6202–6212.

7. Jensen, M. K.; Khaliullin, R.; Schieber, J. D. Self-consistent Modeling of Entangled Network Strands and Linear Dangling Structures in a Single-strand Mean-field Slip-link Model. *Rheologica Acta* **2012**, *51*, 21–35.

8. Chantawansri T.; Sliozberg Y.; Andzelm J. *Linear Viscoelastic Predictions Using a Single-Chain Mean-field Discrete Slip-link Model*; ARL-TR-5295; U.S. Army Research Laboratory: Aberdeen Proving Ground, MD, 2010.

9. Baumgaertel M.; Schausberger A.; Winter H. The Relaxation of Polymers with Linear Flexible Chains of Uniform Length. *Rheologica Acta* **1990**, *29* (5), 400–408.

10. Ressia, J. A.; Villar, M. A.; Valles, E. M. Influence of Polydispersity on the Viscoelastic Properties of Linear Polydimethylsiloxanes and Their Binary Blends. *Polymer* **2000**, *41*, 6885–6894.

11. Rubinstein, M.; Colby, R. H. *Polymer Physics*; Oxford University Press, 2003.

12. Sliozberg, Y. R.; Mrozek, R. A.; Schieber, J. D.; Kröger, M.; Lenhart, J. L.; Andzelm, J. W. Effect of Polymer Solvent on the Mechanical Properties of Entangled Polymer Gels: Coarse-Grained Molecular Simulation. *Polymer* **2013**.

List of Symbols, Abbreviations, and Acroynms

BSW	Baumgaertel, Schausberger, and Winter
CD	constraint dynamics
DSM	discrete slip-link model
ENC	entangled network chain
ESC	entangled solvent chain
IEN	ideal entangled network
NC	network chain
PDMS	polydimethylsiloxane
SC	solvent chain
SD	sliding dynamics

NO. OF COPIES	ORGANIZATION
1 (PDF)	DEFENSE TECHNICAL INFORMATION CTR DTIC OCA
2 (PDF)	DIRECTOR US ARMY RESEARCH LAB RDRL CIO LL IMAL HRA MAIL & RECORDS MGMT
1 (PDF)	GOVT PRINTG OFC A MALHOTRA
4 (PDF)	DIRECTOR US ARMY RESEARCH LAB RDRL WMM G YELENA R SLIOZBERG JAN W ANDZELM JOSEPH L LENHART RANDY A MROZEK
2 (PDF)	ILLINOIS INSTITUTE OF TECHNOLOGY DEPARTMENT OF PHYSICS MARIA KATZAROVA JAY D SCHIEBER 3440 S DEARBORN STREET CHICAGO IL 60616

INTENTIONALLY LEFT BLANK.